Chinese Journal of Catalysis 43 (2022) 1991–2000

available at www.sciencedirect.com

ScienceDirect

journal homepage: www.sciencedirect.com/journal/chinese-journal-of-catalysis

Review

Selectivity control in alkyne semihydrogenation: Recent experimental and theoretical progress

Xiao-Tian Li, Lin Chen, Cheng Shang, Zhi-Pan Liu *

Collaborative Innovation Center of Chemistry for Energy Material, Shanghai Key Laboratory of Molecular Catalysis and Innovative Materials, Key Laboratory of Computational Physical Science, Department of Chemistry, Fudan University, Shanghai 200433, China

ARTICLE INFO

Article history:
Received 30 November 2021
Accepted 24 January 2022
Available online 20 June 2022

Keywords:
Alkyne semihydrogenation
Catalytic selectivity
Surface science
Machine learning
Neural network potential

ABSTRACT

Researchers have been attempting to characterize heterogeneous catalysts *in situ* in addition to correlating their structures with their activity and selectivity in spite of many challenges. Here, we review recent experimental and theoretical advances regarding alkyne selective hydrogenation by Pd-based catalysts, which are an important petrochemical reaction. The catalytic selectivity for the reaction of alkynes to alkenes is influenced by the composition and structure of the catalysts. Recent progress achieved through experimental studies and atomic simulations has provided useful insights into the origins of the selectivity. The important role of the subsurface species (H and C) was revealed by monitoring the catalyst surface and the related catalytic performance. The atomic structures of the Pd catalytic centers and their relationship with selectivity were established through atomic simulations. The combined knowledge gained from experimental and theoretical studies provides a fundamental understanding of catalytic mechanisms and reveals a path toward improved catalyst design.

1. Introduction

As light alkenes are used extensively as chemical building blocks, the selective hydrogenation of alkynes to alkenes is an extremely important petrochemical catalytic process [1–8]. Notably, hydrogenation of the C_2 alkyne (acetylene, CHCH) has attracted the most academic interest owing to its simplicity in illustrating hydrogenation selectivity [9–17]. Although many hydrogenation catalysts can easily convert acetylene to ethene (CH_2CH_2), they often have poor selectivity, which results in the further hydrogenation of ethene to the undesired ethane (CH_3CH_3). Ethene streams produced by naphtha cracking in the petroleum industry typically contain ~1% acetylene, which can poison the downstream catalyst. Therefore, the acetylene needs to be removed or reduced to be less than the 10^{-6} level [9,11,18]. This requires catalysts with high conversion and selectivity for acetylene hydrogenation in excess ethene. A reliable catalyst for industrial applications should satisfy the following four requirements:

(1) higher than 99% conversion of acetylene for purification where acetylene concentrations are below 5×10^{-6},

(2) higher than 80% selectivity for ethene (to improve the economic effectiveness),

(3) $p(C_2H_4):p(C_2H_2) > 20$ for hydrogenation of acetylene in a large excess of ethene, and

(4) reaction temperatures below 100 °C (to reduce the cost).

The search for superior heterogeneous catalysts is of great significance to industry and is an extremely interesting re-

* Corresponding author. E-mail: zpliu@fudan.edu.cn
This work was supported by the National Key Research and Development Program of China (2018YFA0208600) and the National Natural Science Foundation of China (22033003, 21533001, 91745201).
DOI: 10.1016/S1872-2067(21)64036-6 | http://www.sciencedirect.com/journal/chinese-journal-of-catalysis | Chin. J. Catal., Vol. 43, No. 8, August 2022

search hotspot for those in academia.

As early as 1945, Sheridan [19–22] noted the high potential of Pd to act as a catalyst for the selective hydrogenation of acetylene at low temperatures compared to that of Ni, Pt, Rh, and Ir. Later, Frevel *et al*. [23] recognized that alloys of Pd and Ag can significantly improve the selectivity, and Pd-Ag alloys remain the industrial catalyst of choice to date [24–27]. Thereafter, significant efforts were devoted to the search for a superior element to alloy with Pt. However, little progress has been made. A number of alloys, including Pd-Ga [28–31], Pd-In [32–34], Pd-Zn [35–37], Pd-Cu [38,39], and Pd-Au [40–42], have been reported to exhibit better selectivity than the pure Pd catalyst. Although many catalysts exhibit similar performances, none surpass the Pd-Ag alloy.

Along with ongoing efforts to advance catalyst development, the hydrogenation mechanism has been investigated using different experimental techniques and, more recently, theoretical simulations. The fundamental knowledge gained in these studies provides a solid basis for optimizing the selectivity and guiding catalyst design. To date, it has been established that the late transition metal Pd with unsaturated *d*-band states can moderately adsorb H_2 and hydrocarbons, which is the key to its exceptional catalytic ability in hydrogenation reactions [1,7,43,44]. The utilization of Pd to selectively facilitate acetylene hydrogenation while inhibiting ethene hydrogenation, however, poses a much greater challenge and has attracted significant research interest. A widely accepted view is that the good selectivity of Pd originates from subtle differences in the adsorption heat of acetylene and ethene. The Pd surface ensembles promote different adsorption modes for acetylene and ethene and thus achieve high selectivity [1,9,15,44]. Accordingly, modern experimental techniques and theoretical calculations have been utilized to detect and identify the *in situ* surface structures of catalysts and analyze the reaction kinetics.

This review provides an overview of the current understanding of the mechanism of acetylene (or alkyne) selective hydrogenation, mostly with respect to Pd catalysis, obtained from surface science studies and atomic simulations. We will first give a brief explanation of the reaction network and state-of-the-art catalysts, and then discuss the dependence of the hydrogenation selectivity on the catalyst structures. Finally, the outlook is summarized.

2. Reaction network and selectivity

During the manufacturing of polymer-grade ethene, the ethene stream from naphtha cracking often mixes with a small volume of acetylene (approximately 0.5%–2.0%), which can subsequently poison the Ziegler-Natta catalyst for the downstream polymerization reaction. Thus, the volume of acetylene in the ethene stream should be reduced to below 5×10^{-6} [7,9,11,18]. Pd-Ag catalysts are used in industry to remove acetylene by selective hydrogenation to ethene [7,9,11,18], which can be performed under two different hydrogenation conditions, referred to as front-end and tail-end, depending on the position of the hydrogenation reactor in relation to the de-methanizer units. The former condition has a complex feed gas composition containing 10%–35% hydrogen, while the latter, after purification, contains mostly C_2 hydrocarbons and only a limited volume of hydrogen (1%–4%) [7,9,11,18].

Fig. 1 shows the complete reaction network for acetylene hydrogenation proposed by Vignola *et al*. [45] based on density functional theory (DFT) calculation results for Pd(111). The reactions are classified into different types (different colors), and their activation energies are indicated by the size of the arrows/lines. As indicated by the blue arrows, acetylene semihydrogenation closely follows the Horiuti-Polanyi mechanism [46], which involves sequential hydrogenation to vinyl ($CHCH_2$) and ethene. However, the generated ethene, together with the inflow excess ethene can be subject to over-hydrogenation, which results in the undesirable production of ethyl (CH_2CH_3) and ethane. In addition to direct hydrogenation, isomerization may also occur (see the red arrows), resulting in asymmetric C_2 species (CCH_2, CCH_3, and $CHCH_3$), which can lead to the formation of ethane. Moreover, there is a significant risk of coupling between two adjacent C_2 species, especially the easily adsorbed acetylene, vinylidene, and vinyl (oligomerization, indicated by the green arrows). This process results in the formation of C_4 and even higher hydrocarbons (the so-called green oil), which can eventually block the Pd sites and cause catalyst deactivation [10,47]. In summary, both over-hydrogenation and oligomerization can compete with acetylene semihydrogenation, leading to poor selectivity.

The rate of over-hydrogenation and oligomerization depends largely on the H_2 partial pressure in the feed gas, which differs significantly depending on the condition (front-end or tail-end). Catalysis experiments have shown that C–C coupling can only occur in the presence of H_2 [48,49]. The formation of green oil increases with the H_2:C_2H_2 ratio at low H_2 pressures (< 0.1 atm) [50], and then decreases at higher H_2 pressures [49,51]. It is generally accepted that, although the adsorbed H participates in C–C coupling [45,52], it also inhibits the coupling at high H coverage by isolating the adsorbed C_2 species. There-

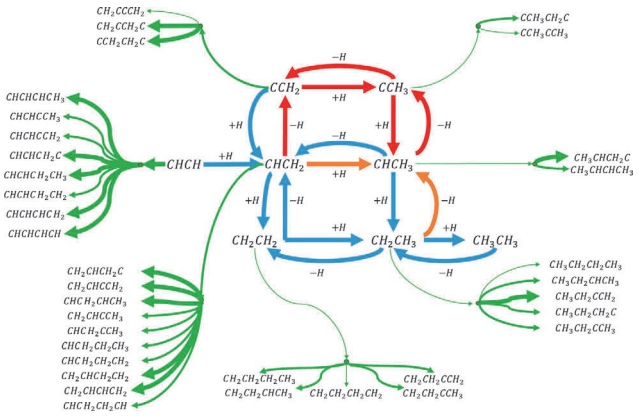

Fig. 1. Reaction network for acetylene hydrogenation. Blue arrows indicate the direct hydrogenation of acetylene and ethene, red arrows indicate isomerization to the asymmetric C_2 species, while the green arrows indicate oligomerization to the C_4 species. Arrows and lines of different sizes represent the different activation energies for the reactions (E_a < 1.5 eV for bold arrow, 1.5 eV < E_a < 2 eV for medium arrow, and E_a > 2 eV for thin arrow). Reproduced with permission [45]. Copyright 2018, American Chemical Society.

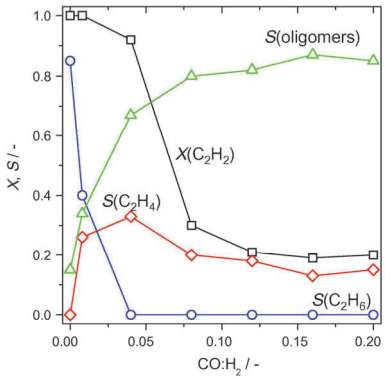

Fig. 2. Conversion (X) of acetylene and selectivity (S) for ethene, ethane, and oligomers over a Pd/γ-Al_2O_3 catalyst as a function of the CO:H_2 ratio Acetylene hydrogenation conditions: $p(C_2H_2)$ = 0.025 bar, $p(H_2)$ = 0.125 bar, p(total) = 1 bar, T = 75 °C, SV = 16800 mL g^{-1} h^{-1}. Reproduced with permission [54]. Copyright 2010, Elsevier.

fore, under the H_2 rich front-end conditions, oligomerization is limited and over-hydrogenation is severe, while the opposite occurs during the tail-end process [18].

3. Modifiers to improve selectivity

3.1. Carbon monoxide as an additive

Because of the fierce competition from over-hydrogenation and oligomerization, the presence of modifiers is imperative to improve the catalytic selectivity. A widely used approach is the addition of a small volume of carbon monoxide to the feed gas [10,12,53–55]. Fig. 2, from a study by García-Mota *et al.* [54], illustrates the effect of CO on the selectivity for acetylene hydrogenation. With an increase in p(CO), the over-hydrogenation sharply reduces and completely stops when $p(CO):p(H_2) > 0.05$. Simultaneously, however, oligomerization increases and the acetylene conversion decreases, both of which are undesirable. Therefore, the CO content should be carefully regulated to allow a compromise between the conversion and selectivity.

It is likely that CO can adsorb competitively with ethene [56] and H [57], and can poison the active Pd sites. In this case, the hydrogenation of both acetylene and ethene is inhibited, especially the latter, because of its weaker adsorption. In addition, the adsorbed CO reduces the number of available Pd sites for the formation of vinylidene, which has been demonstrated to be a precursor of ethane in a labelling study [58]. However, the introduction of CO can also lead to the insertion of CO into the oligomers to form carboxylic acids, thus increasing the oligomerization, as revealed by infrared and nuclear magnetic resonance analyses [59].

3.2. Promoters and state-of-the-art catalysts

Another strategy to improve the selectivity is the proper incorporation of the promoting components in the catalyst. Many Pd alloys have been proven to have better selectivity than pure Pd (Table 1). The benefits of alloying are predominantly attributed to three factors: (1) the promoters can block over-active Pd sites to prevent unwanted ethene hydrogenation [10,12,13], (2) the alloying prevents the formation of the β-PdH phase, which has poor ethene selectivity [7,10,11], and (3) ethene hydrogenation and oligomerization are believed to occur on large Pd ensembles (involving many Pd sites), and thus are inhibited on alloy surfaces where Pd sites are dispersed [12].

Table 1 lists the state-of-the-art catalysts reported in recent years for selective acetylene hydrogenation. As shown, traditional alloy catalysts are still the most popular option. Notably, only a few catalysts satisfy the low-temperature criterion (4) described in the Introduction, and all of them are Pd-based catalysts. This explains why Pd, despite its high cost, is preferred over Cu [3,60,61] and Au [62–64], both of which have high selectivity but are only functional at high temperatures (> 150 °C, Table 1).

4. Insights into selectivity from surface chemistry

In this section, we provide an overview of the key progress toward an understanding of the selectivity. Decades of research have led to the conclusion that the variations in selectivity during hydrogenation are caused by variations in the catalyst structure. This dynamic structural evolution could be a result of the gradual accumulation of adsorbates on the catalyst surface or their penetration into deeper layers [9–11,15]. Experimental studies and theoretical simulations have been performed to detect and identify the catalyst surface structure and thus provide insights into the dependence of selectivity on the catalyst structure.

4.1. Subsurface H and Pd-H phases

Freund *et al.* [26,86–89] performed a series of surface science experiments to investigate alkyne/alkene hydrogenation. By employing temperature-programmed desorption (TPD) under low-pressure conditions (< 10^{-5} mbar), they observed that the hydrogenation of alkenes (including ethene and different isomers of pentene) occurred on Pd/Al_2O_3, but not on Pd(111) single crystals [87,88]. Fig. 3 shows that D_2 produced more TPD desorption peaks in the temperature range of −73–27 °C on Pd/Al_2O_3 than on Pd(111), which is consistent with the quantity of weakly bound subsurface H. As the desorption temperature of subsurface H coincides with that of pentane (Fig. 3(b)), Freund *et al.* [88] proposed that the presence of subsurface H is critical for alkene hydrogenation. They theorized that more active subsurface H is accessible and participates in alkene hydrogenation when the Pd nanoparticles are small (~5 nm), considering that the presence of subsurface H in Pd(111) also exists in experiments [90].

In accordance with Freund group's observation, some other groups [11,91,92] reported that β-PdH (H:Pd > 0.6) has far poorer selectivity than α-PdH (H:Pd ~0.03) for acetylene hydrogenation. For example, Fig. 4 shows experimental results reported by Liu *et al.* [92] for a Pd/C catalyst, which reveal that the selectivity for acetylene over ethene suddenly decreases at

Table 1
State-of-the-art catalysts for the selective hydrogenation of acetylene and their reaction parameters: conversion of acetylene (*X*), selectivity to ethene (*S*), feed gas (C_2H_2:H_2:C_2H_4), space velocity (*SV*), and reaction temperature (*T*).

Type	Catalyst	*X* (%)	*S* (%)	C_2H_2:H_2:C_2H_4	SV (mL g^{-1} h^{-1})	*T* (°C)	Ref.
Pure metal	Tetra-Pd/MgAl-LDHs	93	53	0.3:0.6:32.9	10056	100	[65]
	Ga_2O_3-Pd/Al_2O_3	77	54	0.3:0.6:33.1	17060	100	[66]
	Cu/Al_2O_3	100	84	1:10:50	8×10^5	179	[61]
	Au/SiO_2	82	78	0.8:16:83.2	92000	225	[62]
Alloy & intermetallics	$PdAg_4$	85	49	0.5:5:50	9000	200	[67]
	$PdAg_3$/$MgAl_2O_4$	95	55	0.5:10:50	40000	200	[68]
	$PdAg_3$/r-TiO_2	96	85	0.5:5:50	9.6×10^6	80	[27]
	PdGa/Al_2O_3	83.9	82	0.5:5:50	24000	200	[31]
	Pd_2Ga/CNT	90	58.1	0.5:5:50	7.5×10^6	200	[67]
	PdIn/$MgAl_2O_4$	96	92	0.5:5:50	2.88×10^5	90	[33]
	PdIn/Al_2O_3	100	77	0.87:3.1:73	—	120	[34]
	Pd-Zn/ZnO	94	90	2:20:40	1.8×10^5	80	[35]
	PdZn@ZIF-8C	70	80	0.65:5:50	48000	115	[36]
	$PdBi_3$/Calcite	100	99	1:20:20	1.2×10^5	150	[69]
	Pd@C/CNF	100	93	0.6:1.2:5.4	2.4×10^5	250	[70]
	Pd_4S/CNF	100	95	0.6:1.08:5.4	60000	250	[71]
	Ni_3Ga/$MgAl_2O_4$	90	77	0.5:10:50	40000	200	[68]
	Ni_3Ga-MIHMs	83	80	0.65:5:50	48000	125	[72]
	NiGa/MgAl-LDHs	73	75	1:10:20	1.44×10^5	185	[73]
	Ni_3Sn_2/$MgAl_2O_4$	80	80	0.5:10:50	40000	200	[68]
	$Ni_3ZnC_{0.7}$/oCNT	99	94	0.5:4.5:20	—	200	[74]
	NiCu/CeO_2	100	52.1	0.6:2.4:5.4	98500	—	[75]
	$Al_{13}Fe_4$	80	84	0.5:5:50	90000	200	[4]
	$Co_2Mn_{0.5}Fe_{0.5}Ge$	100	90	0.1:40:10	4500	250	[76]
Coreshell	Pd@H-Zn/Co-ZIF	80	80	0.5:5:50	—	50	[77]
	Pd/CTS	100	74	1:2:20	90000	100	[78]
	Pd/PPS	100	74	0.6:0.9:49.3	28800	100	[79]
Single atom	Pd_1/ND@G	100	90	1:10:20	60000	180	[80]
	Pd_1/MPNC	83	82	0.5:5:50	2.42×10^5	110	[81]
	$AgPd_{0.01}$/SiO_2	67	87	1:20:20	60000	160	[82]
	$CuPd_{0.006}$/SiO_2	100	85	1:20:20	60000	160	[39]
	Na-Ni@CHA	100	90	0.5:8:50	15000	170	[83]
	Cu_1/ND@G	95	98	1:10:20	3000	200	[60]
	Cu_1/Al_2O_3	100	91	1:10:50	8×10^5	188	[61]
Metallic oxide	CeO_2	86	81	1:30:0	—	250	[84]
	In_2O_3	100	85	1:30:0	—	350	[85]

$p(H_2)$ = 0.10 atm at the same time as the α-PdH to β-PdH phase transition [93–95]. They attributed the change in selectivity to the phase transition, which caused Pd lattice expansion. For example, X-ray diffraction by Maeland *et al*. [96] revealed that, along with the α-$PdH_{0.03}$ to β-$PdH_{0.6}$ transformation, the lattice expands from 3.889 to 4.018 Å. Similarly, using DFT calculations, Liu *et al*. [92] found that the absorbed bulk H in β-PdH caused significant expansion of the fcc lattice of Pd from 3.94 to 4.10 Å (DFT typically overestimates the lattice by 1.5%). Lattice expansion enhances the adsorption of ethene on the (100) plane and promotes its hydrogenation, thus decreasing the selectivity.

4.2. Subsurface C and Pd-C phase

It is also likely that, in addition to the subsurface/bulk H, the accumulated carbonaceous deposits can also alter the hydrogenation selectivity via the formation of a surface Pd-C phase

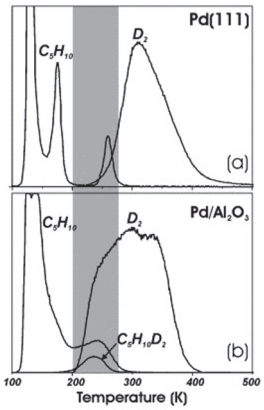

Fig. 3. TPD results for Pd/Al_2O_3 nano-catalyst and Pd(111) single crystal. Desorption peaks for C_5H_{10} and D_2 after their individual adsorption, and desorption peak for $C_5H_{10}D_2$ after co-adsorption of C_5H_{10} and D_2 on Pd(111) (a) and on Pd/Al_2O_3 (b). Reprinted with permission from Ref. [88]. Copyright 2004, Elsevier.

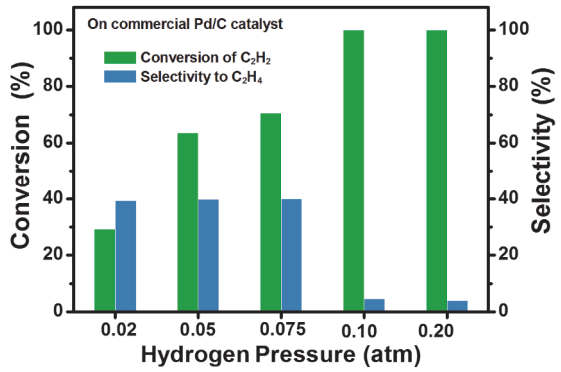

Fig. 4. Sharp decrease in catalytic selectivity along with the α-PdH to β-PdH transition during the acetylene hydrogenation on a Pd/C catalyst Reprinted with permission from Ref. [92]. Copyright 2020, American Chemical Society.

over a long reaction time (> 1 h) [2,9–11,70,74,97,98]. Using *in situ* X-ray photoelectron spectroscopy (XPS), Teschner *et al*. [2,99,100] detected two different surface states with distinct catalytic selectivity, which are formed dynamically under specific reaction conditions (by the modulation of H_2 pressure and temperature). As shown in Fig. 5(a), the selectivity for pentyne over pentene suddenly decreased with an increase in H_2 pressure from 3.5 to 7 mbar [2]. The *in situ* XPS results illustrate that the Pd catalysts contain more high-binding-energy Pd at 3.5 mbar H_2 pressure than at 7.5 mbar (Figs. 5(b,c)), indicating the formation of a surface Pd-C phase. Teschner *et al*. believed this occurred because the surface Pd-C layers can hinder the transport of subsurface H to the surface for alkene hydrogenation, thus improving the selectivity [100]. Remarkably, a spontaneous fluctuation in selectivity was observed at $p(H_2)$ = 0.91 bar (T = 28–30 °C), when the hydrogenation product switched from pentene to pentane [2]. This indicates reversibility in the formation of the metastable surface Pd-C phase. To date, the formation mechanism of the surface Pd-C phase in Pd catalysts remains unclear.

4.3. Pd-Ag surface segregation

The formation of Pd-C and Pd-H phases is generally suppressed by alloying Pd. Thus, the surface status of Pd alloy catalysts plays an important role in controlling the selectivity and warrants further investigation. The Pd-Ag alloy forms a face-centered cubic solid solution at all compositions when it is annealed below ~900 °C [101], in which Ag is known to be enriched on the surface because it has lower surface energy than Pd [102,103]. A recently developed machine learning atomic simulation, specifically the stochastic surface walking-based neural network potential (SSW-NN) [104–113], provides a convenient for the rapid exploration of the complex structure and reaction space in heterogeneous catalysis. Using SSW-NN [104–113], Liu *et al*. [27] demonstrated that the surface segregation of the Pd-Ag catalyst can be modulated by adjusting the reaction conditions (Fig. 6): Ag-exposed surfaces are dominant in the absence of H_2, whereas Pd-exposed surfaces, particularly the (111) surface, are thermodynamically favorable at high H_2 pressure in the presence of surface-adsorbed H, as Pd-H interactions are stronger than those of Ag-H. The surfacing of Pd atoms results in the formation of Pd-line, Pd-triangle, and Pd-dimer ensembles at the surface layer during hydrogenation. The H atoms are adsorbed at these Pd sites, which are either hollow sites or bridge sites. However, because the open (100) surface has a higher surface energy, Ag atoms can cover the (100) surface and block the hydrogenation reaction even under hydrogenation conditions. This is a major cause of the high selectivity of the Pd-Ag alloy, because the side reactions, ethene hydrogenation and C–C coupling, both have low barriers (0.89 and 1.08 eV, respectively [92]) on the Pd(100) surface.

4.4. Important role of adsorption energy

Nørskov *et al*. [1,44] observed that the adsorption energy can be used to explain the relationship between the selectivity and catalyst structure. For a good catalyst, an appreciable quantity of adsorption energy is required to favor acetylene hydrogenation, while the ethene adsorption energy should be as small as possible to enable rapid ethene desorption. Using DFT calculations, Nørskov *et al*. [1] found that the adsorption strengths of acetylene, ethene, and methyl are closely correlated because of their similar surface binding modes. Acetylene,

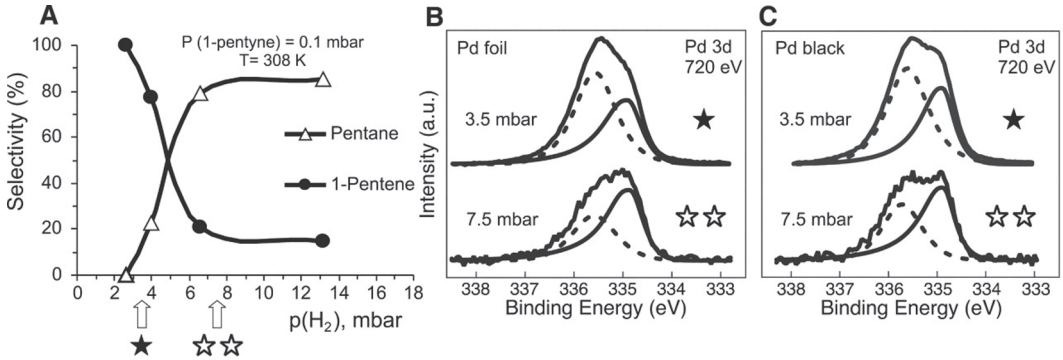

Fig. 5. (a) Catalytic selectivity as a function of H_2 pressure in 1-pentyne hydrogenation on Pd black catalyst. (b,c) Corresponding Pd $3d_{5/2}$ XPS recorded at distinct H_2 pressures (as marked by solid and open stars in (a)), over the Pd foil and the Pd black catalysts. The XPS peaks at 335 eV (solid line) correspond to metallic Pd, while the higher binding-energy peaks (dashed line) are attributed to the sum of adsorbate-induced surface components, especially the Pd-C phase. Reprinted with permission from Ref. [2]. Copyright 2008, the American Association for the Advancement of Science.

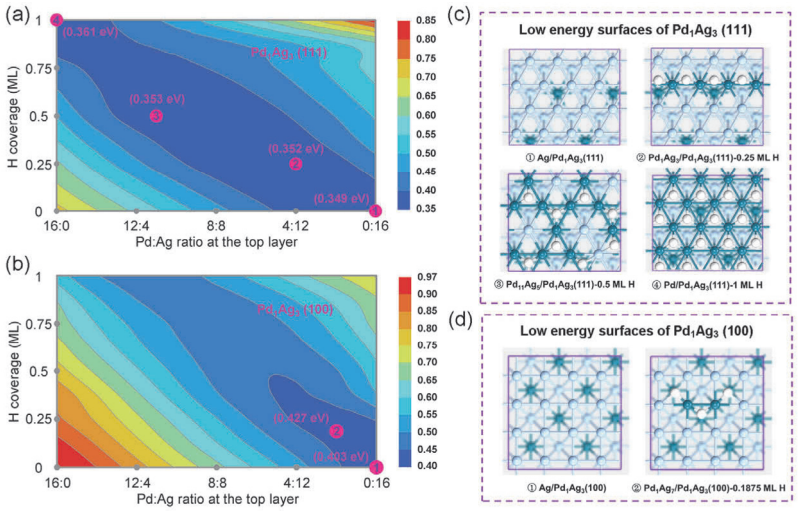

Fig. 6. (a,b) Pd-Ag-H surface contour maps for the formation free energies of Pd-Ag-H/Pd_1Ag_3(111) and Pd-Ag-H/Pd_1Ag_3(100), respectively, at 25 °C and $p(H_2)$ = 0.05 atm. (c,d) Stable surface configurations of Pd_1Ag_3(111) and Pd_1Ag_3(100), respectively, under typical reaction conditions, as identified from the Pd-Ag-H surface contour maps. Reprinted with permission from Ref. [27]. Copyright 2021, American Chemical Society.

ethene, and methyl can form 4, 2, and 1 σ bonds, respectively, when adsorbed on the surface, leading to a scaling trend for their adsorption energies (Fig. 7). Thus, an energy window was identified to allow for a compromise between the activity and selectivity. With reference to this window, the non-precious metal Ni-Zn alloy was selected as a good candidate for selective acetylene hydrogenation.

Zhang *et al*. [7] also discussed the important role of adsorption energy in determining the hydrogenation selectivity. They concluded that ethene has three adsorption modes on the catalyst surface depending on the Pd ensembles: ethylidyne mode on hollow Pd sites, di-σ-mode on bridge Pd sites, and π-bonded mode on isolated Pd sites. Their adsorption energies decreased in the order of ethylidyne > di-σ > π-bonded. This inspired the design of single-atom catalysts, which cause the π-bonded ethene to easily desorb, leading to good selectivity [7,39,82,114,115]. However, the isolated Pd sites also have poorer activity and appear only to function at high temperatures (> 150 °C, Table 1).

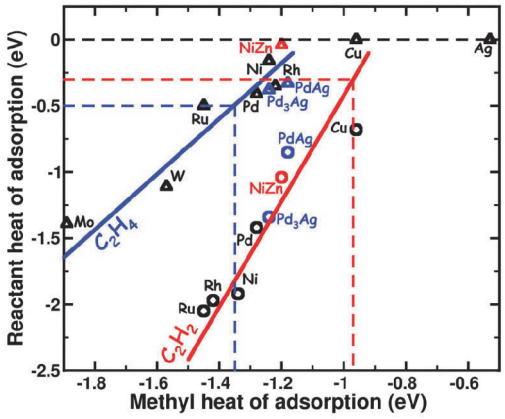

Fig. 7. Adsorption energies of acetylene (circles) and ethene (triangles) plotted against the adsorption energy of methyl. Reprinted with permission from Ref. [1]. Copyright 2008, the American Association for the Advancement of Science.

4.5. *Distinct selectivity of Pd(111) and Pd(100)*

Although the adsorption energies of acetylene and ethene are effective descriptors for selectivity, their computation relies heavily on pre-knowledge of the catalyst structure. More importantly, these thermodynamic descriptors cannot provide accurate reaction kinetics for catalyst optimization. Facilitated by the rapid structure and reaction exploration of the SSW-NN

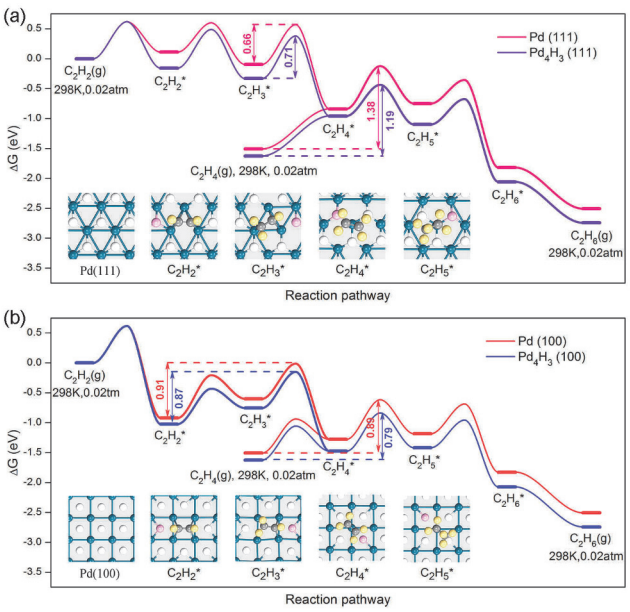

Fig. 8. Gibbs free energy profiles for acetylene hydrogenation on (a) Pd(111), Pd_4H_3(111), (b) Pd(100), and Pd_4H_3(100). Pd and Pd_4H_3 are the detailed structures for α-PdH and β-PdH as determined by SSW-NN global optimization. The insets show the intermediates during the hydrogenation reactions. Color code: H atoms of adsorbates, yellow balls; H atoms bonded to adsorbates, pink balls; other H atoms, white balls; Pd atoms, indigo balls; and C atoms, gray balls). Reprinted with permission from Ref. [92]. Copyright 2020, American Chemical Society.

method [104–113], Liu *et al*. [27,92] investigated acetylene hydrogenation on pure Pd (Fig. 8) and Pd-Ag (Fig. 6) catalysts by combining theoretical calculations and catalysis experiments. They found that at high acetylene conversions (such as those under H_2 rich front-end conditions), H atoms tend to cover both Pd(111) and Pd(100) (ΔG_{ads} = –0.2––0.3 eV) in a complete monolayer due to the weak H–H interactions. Owing to the high H coverage, the adsorption of acetylene is significantly reduced, from –1.91 to –0.51 eV on the Pd(111) surface, as is the risk of C-C coupling (oligomerization). Furthermore, ethene adsorption is significantly reduced on the close-packed (111) surface, which lifts the hydrogenation barriers for the conversion of ethene to ethane to approximately 1.19–1.38 eV, and effectively prevents deep hydrogenation. However, on the open (100) surface, the repulsion due to the pre-adsorbed H is moderate and ethene hydrogenation can still proceed with a barrier of approximately 0.79–0.89 eV, which causes the poor selectivity of pure Pd. This finding is consistent with the theoretical results obtained by Grönbeck *et al*. [116] and Zhou *et al*. [117].

Considering that (111) and (100) are the two lowest-surface-energy facets, and both exist in large quantities in real Pd nanoparticles (for example, (111):(100) ≈ 9:1) [87,92], Liu *et al*. proposed a straightforward strategy to improve the selectivity, which involves blocking the non-selective (100) facets. The tetrahedral Pd nanoparticles [65] and the Ga_2O_3-deposited Pd catalyst [66], in which most of the (111) plane is exposed, have comparable selectivity to some of the alloy catalysts (Table 1). Similarly, the success of the Pd-Ag alloy catalyst can be largely attributed to the tendency for Ag to cover the (100) plane. By further adjusting the Pd:Ag ratios, Liu *et al*. [27] determined Pd:Ag = 1:3 to be the optimum ratio for the Pd-Ag alloy, as it maximizes the quantity of Ag that blocks the (100) plane and results in a significant fraction of Pd exposed on (111) to catalyze the selective hydrogenation (Fig. 6). Finally, a Pd_1Ag_3 alloy supported on rutile-TiO_2, which achieves a high selectivity (> 85%) at high acetylene conversion (> 96%), was selected. This combinational experiment-and-theory investigation demonstrates how a deep understanding of the catalyst structure and reaction mechanism can facilitate the rational design of improved catalysts.

5. Summary and outlook

In this review, we summarized recent advances toward improved selectivity control of alkyne hydrogenation by Pd-based catalysts, especially with respect to acetylene hydrogenation. The review is organized into three sections, covering the reaction network, reaction conditions, and catalyst structures. Research using modern experimental and theoretical techniques has established that the catalyst surface structures are dynamic under hydrogenation conditions, including Pd-H, Pd-C phases, and different compositions in Pd-M alloy phases. The catalyst morphology and surface status, which are controlled by the synthesis and reaction conditions, determine the catalytic selectivity, largely by influencing the adsorption energies of acetylene and ethene on the Pd sites. While substantial progress has been achieved, important challenges remain, some of which are highlighted below.

(1) The oligomerization (C-C coupling) reaction mechanism and the active Pd sites are still unclear. Further studies are required to probe the formation mechanism of the surface Pd-C phase and the oligomerization kinetics.

(2) Synthetic methods for accurately controlling the catalyst morphology and local Pd ensembles need to be developed to better control the selectivity. In particular, controlling the (100):(111) ratio for supported Pd_1Ag_3 catalysts remains a challenge.

(3) A low-temperature catalyst without Pd remains unavailable. Ni-based catalysts cannot function below 100 °C. New architectures for low-temperature hydrogenation catalysts using non-precious elements are highly desirable.

The machine learning potential method, as demonstrated by the global neural network implemented in the large-scale atomic simulation with neural network potential (LASP) program, can overcome the current limitations in the time scale and the system size of the atomic simulation. By integrating with other simulation techniques, theoretical simulations should be applicable to more complicated problems such as dynamic structure evolution, the search for complex reaction networks, and long-time molecular dynamic simulations in large systems. This will eventually benefit the rational design of better catalysts for important catalytic transformations, including the alkyne selective hydrogenation discussed herein.

References

[1] F. Studt, F. Abild-Pedersen, T. Bligaard, R. Z. Sørensen, C. H. Christensen, J. K. Nørskov, *Science*, **2008**, 320, 1320–1322.

[2] D. Teschner, J. Borsodi, A. Wootsch, Z. Révay, M. Hävecker, A. Knop-Gericke, S. D. Jackson, R. Schlögl, *Science*, **2008**, 320, 86–89.

[3] G. Kyriakou, M. Boucher, A. Jewell, E. Lewis, T. Lawton, A. Baber, H. Tierney, M. Flytzani-Stephanopoulos, E. C. H. Sykes, *Science*, **2012**, 335, 1209–1212.

[4] M. Armbrüster, K. Kovnir, M. Friedrich, D. Teschner, G. Wowsnick, M. Hahne, P. Gille, L. Szentmiklósi, M. Feuerbacher, M. Heggen, F. Girgsdies, D. Rosenthal, R. Schlögl, Y. Grin, *Nat. Mater.*, **2012**, 11, 690–693.

[5] Q.-A. Chen, Z.-S. Ye, Y. Duan, Y.-G. Zhou, *Chem. Soc. Rev.*, **2013**, 42, 497–511.

[6] S. Wei, A. Li, J. Liu, Z. Li, W. Chen, Y. Gong, Q. Zhang, W.-C.M. Cheong, Y. Wang, L. Zheng, H. Xiao, C. Chen, D. Wang, Q. Peng, L. Gu, X. Han, J. Li, Y. Li, *Nat. Nanotechnol.*, **2018**, 13, 856–861.

[7] L. Zhang, M. Zhou, A. Wang, T. Zhang, *Chem. Rev.*, **2020**, 120, 683–733.

[8] J. Bu, Z. Liu, W. Ma, L. Zhang, T. Wang, H. Zhang, Q. Zhang, X. Feng, J. Zhang, *Nat. Catal.*, **2021**, 4, 557–564.

[9] A. N. R. Bos, K. R. Westerterp, *Chem. Eng. Process. Process Intensif.*, **1993**, 32, 1–7.

[10] Á. Molnár, A. Sárkány, M. Varga, *J. Mol. Catal. A*, **2001**, 173, 185–221.

[11] A. Borodziński, G. C. Bond, *Catal. Rev. Sci. Eng.*, **2006**, 48, 91–144.

[12] A. Borodziński, G. C. Bond, *Catal. Rev. Sci. Eng.*, **2008**, 50, 379–469.

[13] S. A. Nikolaev, L. N. Zanaveskin, V. V. Smirnov, V. A. Averyanov, K. L. Zanaveskin, *Russ. Chem. Rev.*, **2009**, 78, 231–247.

[14] N. López, C. Vargas-Fuentes, *Chem. Commun.*, **2012**, 48,

Graphical Abstract

Chin. J. Catal., 2022, 43: 1991–2000 doi: 10.1016/S1872-2067(21)64036-6

Selectivity control in alkyne semihydrogenation: Recent experimental and theoretical progress

Xiao-Tian Li, Lin Chen, Cheng Shang, Zhi-Pan Liu *
Fudan University

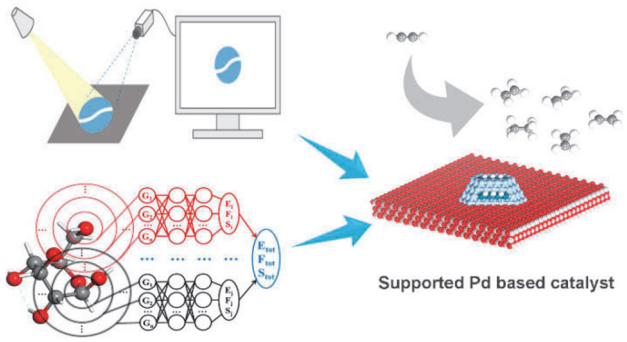

This review summarizes the recent progress in alkyne selective hydrogenation on Pd-based catalysts, especially the understanding of the relationship between catalyst surface structure and catalytic selectivity, as demonstrated by surface science experiments and theoretical simulations.

1379–1391.
[15] M. Armbrüster, M. Behrens, F. Cinquini, K. Föttinger, Y. Grin, A. Haghofer, B. Klötzer, A. Knop-Gericke, H. Lorenz, A. Ota, S. Penner, J. Prinz, C. Rameshan, Z. Révay, D. Rosenthal, G. Rupprechter, P. Sautet, R. Schlögl, L. Shao, L. Szentmiklósi, D. Teschner, D. Torres, R. Wagner, R. Widmer, G. Wowsnick, *ChemCatChem*, **2012**, 4, 1048–1063.
[16] A. J. McCue, J. A. Anderson, *Front. Chem. Sci. Eng.*, **2015**, 9, 142–153.
[17] J. Kammert, J. Moon, Z. Wu, *Chin. J. Catal.*, **2020**, 41, 901–914.
[18] D. C. Huang, K. H. Chang, W. F. Pong, P. K. Tseng, K. J. Hung, W. F. Huang, *Catal. Lett.*, **1998**, 53, 155–159.
[19] J. Sheridan, *J. Chem. Soc.*, **1944**, 373–380.
[20] J. Sheridan, *J. Chem. Soc.*, **1945**, 305–311.
[21] J. Sheridan, *J. Chem. Soc.*, **1945**, 470–476.
[22] J. Sheridan, W. D. Reid, *J. Chem. Soc.*, **1952**, 2962–2966.
[23] L. K. Frevel, L. J. Kressley, US Patent 2802889, **1957**.
[24] Q. Zhang, J. Li, X. Liu, Q. Zhu, *Appl. Catal. A*, **2000**, 197, 221–228.
[25] Y. Jin, A. K. Datye, E. Rightor, R. Gulotty, W. Waterman, M. Smith, M. Holbrook, J. Maj, J. Blackson, *J. Catal.*, **2001**, 203, 292–306.
[26] N. A. Khan, S. Shaikhutdinov, H. J. Freund, *Catal. Lett.*, **2006**, 108, 159–164.
[27] X.-T. Li, L. Chen, C. Shang, Z.-P. Liu, *J. Am. Chem. Soc.*, **2021**, 143, 6281–6292.
[28] J. Osswald, R. Giedigkeit, R. E. Jentoft, M. Armbrüster, F. Girgsdies, K. Kovnir, T. Ressler, Y. Grin, R. Schlögl, *J. Catal.*, **2008**, 258, 210–218.
[29] J. Osswald, K. Kovnir, M. Armbrüster, R. Giedigkeit, R. E. Jentoft, U. Wild, Y. Grin, R. Schlögl, *J. Catal.*, **2008**, 258, 219–227.
[30] M. Armbrüster, K. Kovnir, M. Behrens, D. Teschner, Y. Grin, R. Schlögl, *J. Am. Chem. Soc.*, **2010**, 132, 14745–14747.
[31] M. Armbrüster, G. Wowsnick, M. Friedrich, M. Heggen, R. Cardoso-Gil, *J. Am. Chem. Soc.*, **2011**, 133, 9112–9118.
[32] Y. Luo, S. Alarcón Villaseca, M. Friedrich, D. Teschner, A. Knop-Gericke, M. Armbrüster, *J. Catal.*, **2016**, 338, 265–272.
[33] Q. Feng, S. Zhao, Y. Wang, J. Dong, W. Chen, D. He, D. Wang, J. Yang, Y. Zhu, H. Zhu, L. Gu, Z. Li, Y. Liu, R. Yu, J. Li, Y. Li, *J. Am. Chem. Soc.*, **2017**, 139, 7294–7301.
[34] Y. Cao, Z. Sui, Y. Zhu, X. Zhou, D. Chen, *ACS Catal.*, **2017**, 7, 7835–7846.
[35] H. Zhou, X. Yang, L. Li, X. Liu, Y. Huang, X. Pan, A. Wang, J. Li, T. Zhang, *ACS Catal.*, **2016**, 6, 1054–1061.
[36] M. Hu, S. Zhao, S. Liu, C. Chen, W. Chen, W. Zhu, C. Liang, W.-C. Cheong, Y. Wang, Y. Yu, Q. Peng, K. Zhou, J. Li, Y. Li, *Adv. Mater.*, **2018**, 30, 1801878.
[37] L. Yang, Y. Guo, J. Long, L. Xia, D. Li, J. Xiao, H. Liu, *Chem. Commun.*, **2019**, 55, 14693–14696.
[38] A. J. McCue, C. J. McRitchie, A. M. Shepherd, J. A. Anderson, *J. Catal.*, **2014**, 319, 127–135.
[39] G. X. Pei, X. Y. Liu, X. Yang, L. Zhang, A. Wang, L. Li, H. Wang, X. Wang, T. Zhang, *ACS Catal.*, **2017**, 7, 1491–1500.
[40] C. Ma, Y. Du, J. Feng, X. Cao, J. Yang, D. Li, *J. Catal.*, **2014**, 317, 263–271.
[41] G. X. Pei, X. Y. Liu, A. Wang, L. Li, Y. Huang, T. Zhang, J. W. Lee, B. W. L. Jang, C.-Y. Mou, *New J. Chem.*, **2014**, 38, 2043–2051.
[42] S. Zhang, C.-Y. Chen, B. W. L. Jang, A.-M. Zhu, *Catal. Today*, **2015**, 256, 161–169.
[43] P. A. Sheth, M. Neurock, C. M. Smith, *J. Phys. Chem. B*, **2005**, 109, 12449–12466.
[44] F. Studt, F. Abild-Pedersen, T. Bligaard, R. Z. Sørensen, C. H. Christensen, J. K. Nørskov, *Angew. Chem. Int. Ed.*, **2008**, 47, 9299–9302.
[45] E. Vignola, S. N. Steinmann, A. Al Farra, B. D. Vandegehuchte, D. Curulla, P. Sautet, *ACS Catal.*, **2018**, 8, 1662–1671.
[46] I. Horiuti, M. Polanyi, *Trans. Faraday Soc.*, **1934**, 30, 1164–1172.
[47] M. Larsson, J. Jansson, S. Asplund, *J. Catal.*, **1996**, 162, 365–367.
[48] A. S. Al-Ammar, G. Webb, *J. Chem. Soc., Faraday Trans. 1*, **1978**, 74, 657–664.

[49] G. C. Battiston, L. Dalloro, G. R. Tauszik, *Appl. Catal.*, **1982**, 2, 1–17.
[50] M. Larsson, J. Jansson, S. Asplund, *J. Catal.*, **1998**, 178, 49–57.
[51] Z. E. Gandman, M. E. Aerov, V. A. Men'shchikov, V. S. Getmantsev, *Int. Chem. Eng.*, **1975**, 15, 183–185.
[52] B. Yang, R. Burch, C. Hardacre, P. Hu, P. Hughes, *J. Phys. Chem. C*, **2014**, 118, 1560–1567.
[53] Y. H. Park, G. L. Price, *Ind. Eng. Chem. Res.*, **1991**, 30, 1693–1699.
[54] M. García-Mota, B. Bridier, J. Pérez-Ramírez, N. López, *J. Catal.*, **2010**, 273, 92–102.
[55] D. L. Trimm, I. O. Y. Liu, N. W. Cant, *Appl. Catal. A*, **2010**, 374, 58–64.
[56] I. Ratajczykowa, I. Szymerska, *Chem. Phys. Lett.*, **1983**, 96, 243–246.
[57] A. S. Al-Ammar, G. Webb, *J. Chem. Soc., Faraday Trans. 1*, **1979**, 75, 1900–1911.
[58] J. Margitfalvi, L. Guczi, A. H. Weiss, *React. Kinet. Catal. Lett.*, **1981**, 15, 475–479.
[59] A. Sárkány, A. H. Weiss, T. Szilágyi, P. Sándor, L. Guczi, *Appl. Catal.*, **1984**, 12, 373–379.
[60] F. Huang, Y. Deng, Y. Chen, X. Cai, M. Peng, Z. Jia, J. Xie, D. Xiao, N. Wang, Z. Jiang, H. Liu, D. Ma, *Nat. Commun.*, **2019**, 10, 4431.
[61] X. Shi, Y. Lin, L. Huang, Z. Sun, Y. Yang, X. Zhou, E. Vovk, X. Liu, X. Huang, M. Sun, S. Wei, J. Lu, *ACS Catal.*, **2020**, 10, 3495–3504.
[62] X. Liu, C.-Y. Mou, S. Lee, Y. Li, J. Secrest, B. W. L. Jang, *J. Catal.*, **2012**, 285, 152–159.
[63] X. Yan, J. Wheeler, B. Jang, W.-Y. Lin, B. Zhao, *Appl. Catal. A*, **2014**, 487, 36–44.
[64] X. Yan, J. Bao, C. Yuan, J. Wheeler, W.-Y. Lin, R. Li, B. W. L. Jang, *J. Catal.*, **2016**, 344, 194–201.
[65] J. Feng, X. Ma, Y. He, D.G. Evans, D. Li, *Appl. Catal. A*, **2012**, 413–414, 10–20.
[66] L. Ding, H. Yi, W. Zhang, R. You, T. Cao, J. Yang, J. Lu, W. Huang, *ACS Catal.*, **2016**, 6, 3700–3707.
[67] L. Shao, W. Zhang, M. Armbrüster, D. Teschner, F. Girgsdies, B. Zhang, O. Timpe, M. Friedrich, R. Schlögl, D. Su, *Angew. Chem. Int. Ed.*, **2011**, 50, 10231–10235.
[68] Y. Liu, X. Liu, Q. Feng, D. He, L. Zhang, C. Lian, R. Shen, G. Zhao, Y. Ji, D. Wang, G. Zhou, Y. Li, *Adv. Mater.*, **2016**, 28, 4747–4754.
[69] B. Lou, H. Kang, W. Yuan, L. Ma, W. Huang, Y. Wang, Z. Jiang, Y. Du, S. Zou, J. Fan, *ACS Catal.*, **2021**, 11, 6073–6080.
[70] Y. Liu, F. Fu, A. McCue, W. Jones, D. Rao, J. Feng, Y. He, D. Li, *ACS Catal.*, **2020**, 10, 15048–15059.
[71] A. J. McCue, A. Guerrero-Ruiz, I. Rodríguez-Ramos, J. A. Anderson, *J. Catal.*, **2016**, 340, 10–16.
[72] M. Hu, W. Yang, S. Liu, W. Zhu, Y. Li, B. Hu, Z. Chen, R. Shen, W.-C. Cheong, Y. Wang, K. Zhou, Q. Peng, C. Chen, Y. Li, *Chem. Sci.*, **2019**, 10, 614–619.
[73] Y. Cao, H. Zhang, S. Ji, Z. Sui, Z. Jiang, D. Wang, F. Zaera, X. Zhou, X. Duan, Y. Li, *Angew. Chem. Int. Ed.*, **2020**, 59, 11647–11652.
[74] N. Yiming, X. Huang, Y. Wang, M. Xu, J. Chen, S. Xu, M. G. Willinger, W. Zhang, M. Wei, B. Zhang, *Nat. Commun.*, **2020**, 11, 3324.
[75] Y. Liu, A. J. McCue, P. Yang, Y. He, L. Zheng, X. Cao, Y. Man, J. Feng, J. A. Anderson, D. Li, *Chem. Sci.*, **2019**, 10, 3556–3566.
[76] T. Kojima, S. Kameoka, S. Fujii, S. Ueda, A.-P. Tsai, *Sci. Adv.*, **2018**, 4, eaat6063.
[77] J. Yang, F. Zhang, H. Lu, X. Hong, H.-L. Jiang, Y. Wu, Y. Li, *Angew. Chem. Int. Ed.*, **2015**, 54, 10889–10893.
[78] Q. Guan, C. Yang, S. Wang, L. He, Z. Kong, X. Chai, H. Xin, P. Ning, *ACS Catal.*, **2019**, 9, 11146–11152.
[79] S. Lee, S.-J. Shin, H. Baek, Y. Choi, K. Hyun, M. Seo, K. Kim, D.-Y. Koh, M. Choi, *Sci. Adv.*, **2020**, 6, eabb7369.
[80] F. Huang, Y. Deng, Y. Chen, X. Cai, M. Peng, Z. Jia, P. Ren, D. Xiao, X. Wen, N. Wang, H. Liu, D. Ma, *J. Am. Chem. Soc.*, **2018**, 140, 13142–13146.
[81] Q. Feng, S. Zhao, Q. Xu, W. Chen, S. Tian, Y. Wang, W. Yan, J. Luo, D. Wang, Y. Li, *Adv. Mater.*, **2019**, 31, 1901024.
[82] G. X. Pei, X. Y. Liu, A. Wang, A. F. Lee, M. A. Isaacs, L. Li, X. Pan, X. Yang, X. Wang, Z. Tai, K. Wilson, T. Zhang, *ACS Catal.*, **2015**, 5, 3717–3725.
[83] Y. Chai, G. Wu, X. Liu, Y. Ren, W. Dai, C. Wang, Z. Xie, N. Guan, L. Li, *J. Am. Chem. Soc.*, **2019**, 141, 9920–9927.
[84] G. Vilé, B. Bridier, J. Wichert, J. Pérez-Ramírez, *Angew. Chem. Int. Ed.*, **2012**, 51, 8620–8623.
[85] D. Albani, M. Capdevila-Cortada, G. Vilé, S. Mitchell, O. Martin, N. López, J. Pérez-Ramírez, *Angew. Chem. Int. Ed.*, **2017**, 56, 10755–10760.
[86] S. Shaikhutdinov, M. Heemeier, M. Bäumer, T. Lear, D. Lennon, R. J. Oldman, S. D. Jackson, H. J. Freund, *J. Catal.*, **2001**, 200, 330–339.
[87] A. M. Doyle, S. K. Shaikhutdinov, S. D. Jackson, H.-J. Freund, *Angew. Chem. Int. Ed.*, **2003**, 42, 5240–5243.
[88] A. M. Doyle, S. K. Shaikhutdinov, H. J. Freund, *J. Catal.*, **2004**, 223, 444–453.
[89] M. Wilde, K. Fukutani, W. Ludwig, B. Brandt, J.-H. Fischer, S. Schauermann, H.-J. Freund, *Angew. Chem. Int. Ed.*, **2008**, 47, 9289–9293.
[90] G. E. Gdowski, T. E. Felter, R. H. Stulen, *Surf. Sci.*, **1987**, 181, L147–L155.
[91] A. Borodziński, A. Janko, *React. Kinet. Catal. Lett.*, **1977**, 7, 163–169.
[92] X.-T. Li, L. Chen, G.-F. Wei, C. Shang, Z.-P. Liu, *ACS Catal.*, **2020**, 10, 9694–9705.
[93] J. E. Worsham, M. K. Wilkinson, C. G. Shull, *J. Phys. Chem. Solids*, **1957**, 3, 303–310.
[94] G. Nelin, *Phys. Status Solidi B*, **1971**, 45, 527–536.
[95] L. L. Jewell, B. H. Davis, *Appl. Catal. A*, **2006**, 310, 1–15.
[96] A. J. Maeland, T. R. P. Gibb, *J. Phys. Chem.*, **1961**, 65, 1270–1272.
[97] B. Yang, R. Burch, C. Hardacre, G. Headdock, P. Hu, *J. Catal.*, **2013**, 305, 264–276.
[98] W. Xie, J. Xu, Y. Ding, P. Hu, *ACS Catal.*, **2021**, 11, 4094–4106.
[99] D. Teschner, E. Vass, M. Hävecker, S. Zafeiratos, P. Schnörch, H. Sauer, A. Knop-Gericke, R. Schlögl, M. Chamam, A. Wootsch, A. S. Canning, J. J. Gamman, S. D. Jackson, J. McGregor, L. F. Gladden, *J. Catal.*, **2006**, 242, 26–37.
[100] D. Teschner, J. Borsodi, Z. Kis, L. Szentmiklósi, Z. Révay, A. Knop-Gericke, R. Schlögl, D. Torres, P. Sautet, *J. Phys. Chem. C*, **2010**, 114, 2293–2299.
[101] I. Karakaya, W. T. Thompson, *Bull. Alloy Phase Diagrams*, **1988**, 9, 237–243.
[102] P. T. Wouda, M. Schmid, B. E. Nieuwenhuys, P. Varga, *Surf. Sci.*, **1998**, 417, 292–300.
[103] J. S. Lim, J. Vandermause, M. A. van Spronsen, A. Musaelian, Y. Xie, L. Sun, C. R. O'Connor, T. Egle, N. Molinari, J. Florian, K. Duanmu, R. J. Madix, P. Sautet, C. M. Friend, B. Kozinsky, *J. Am. Chem. Soc.*, **2020**, 142, 15907–15916.
[104] C. Shang, Z.-P. Liu, *J. Chem. Theory Comput.*, **2013**, 9, 1838–1845.
[105] X.-J. Zhang, C. Shang, Z.-P. Liu, *J. Chem. Theory Comput.*, **2013**, 9, 3252–3260.
[106] C. Shang, X.-J. Zhang, Z.-P. Liu, *Phys. Chem. Chem. Phys.*, **2014**, 16, 17845–17856.
[107] S.-D. Huang, C. Shang, X.-J. Zhang, Z.-P. Liu, *Chem. Sci.*, **2017**, 8, 6327–6337.
[108] S.-D. Huang, C. Shang, P.-L. Kang, Z.-P. Liu, *Chem. Sci.*, **2018**, 9, 8644–8655.

[109] S.-D. Huang, C. Shang, P.-L. Kang, X.-J. Zhang, Z.-P. Liu, *Wiley Interdiscip. Rev.-Comput. Mol. Sci.*, **2019**, 9, e1415.
[110] P.-L. Kang, C. Shang, Z.-P. Liu, *J. Am. Chem. Soc.*, **2019**, 141, 20525–20536.
[111] P.-L. Kang, C. Shang, Z.-P. Liu, *Acc. Chem. Res.*, **2020**, 53, 2119–2129.
[112] S. Ma, Z.-P. Liu, *ACS Catal.*, **2020**, 10, 13213–13226.
[113] S. Ma, S.-D. Huang, Z.-P. Liu, *Nat. Catal.*, **2019**, 2, 671–677.
[114] H. Zhou, X. Yang, A. Wang, S. Miao, X. Liu, X. Pan, Y. Su, L. Li, Y. Tan, T. Zhang, *Chin. J. Catal.*, **2016**, 37, 692–699.
[115] G. Pei, X. Liu, M. Chai, A. Wang, T. Zhang, *Chin. J. Catal.*, **2017**, 38, 1540–1548.
[116] M. Jørgensen, H. Grönbeck, *J. Am. Chem. Soc.*, **2019**, 141, 8541–8549.
[117] Y. Cao, W. Fu, Z. Sui, X. Duan, D. Chen, X. Zhou, *Ind. Eng. Chem. Res.*, **2019**, 58, 1888–1895.

调控炔烃半氢化反应的催化选择性：实验和理论的最新进展

李晓天, 陈　林, 商　城, 刘智攀*
复旦大学化学系, 上海市分子催化和功能材料重点实验室, 物质计算科学教育部重点实验室, 上海200433

摘要: 由于短链烯烃的广泛应用, 炔烃选择性加氢制备烯烃是一个非常重要的石油化学催化过程. 其中最简单的乙炔半氢化, 吸引了众多研究者的广泛研究, 是催化选择性调控的一个非常重要反应. 工业上, 由石油蒸汽裂解得到的乙烯往往混有微量(~1%)的乙炔, 它会毒化乙烯聚合反应时所使用的Ziegler-Natta催化剂, 因此需要降低乙炔含量至5×10^{-6}以下. 这要求加氢催化剂具有很高的乙炔转化率(> 99%)和乙烯选择性(> 80%). Pd基催化剂因低温下的具有高活性, 是最常用的炔烃半氢化催化剂, 其中Pd-Ag合金催化剂已在工业界应用了数十年. 近十几年来, 新型的乙炔半氢化催化剂不断被提出, 其催化选择性的研究也取得了很大的进展.

本文对炔烃半氢化反应的最新研究进展进行了总结. 以乙炔加氢为例, 介绍了其工业反应的条件、反应的网络以及潜在的副反应. 归纳了提高加氢选择性的常见方法, 并总结了近十几年报道的性能较好的乙炔半氢化催化剂. 重点阐述了近年研究对加氢选择性的深入理解: Pd基催化剂的表面结构会随着反应条件和反应过程动态变化, 从而影响加氢选择性. 利用程序升温脱附和X射线光电子能谱研究催化剂的表面性质和相应的催化性能, 确认了次表层H和表层C的出现, 并发现了它们对催化选择性的重要影响. 理论模拟(DFT, SSW-NN)建立了催化活性中心的原子结构, 发现了Ag在PdAg合金表面的富集, 以及在反应条件下Pd原子偏析到(111)面, 阐明了晶面结构与催化选择性之间的定量关联. 综上, 实验和理论的结合不仅深化了研究者对加氢选择性的理解, 也为设计更好的催化剂提供了有效的指导.

关键词: 炔烃半氢化; 催化选择性; 表面科学; 机器学习; 神经网络势

收稿日期: 2021-11-30. 接受日期: 2022-01-24. 上网时间: 2022-06-20.
*通讯联系人. 电子信箱: zpliu@fudan.edu.cn
基金来源: 国家重点研发计划(2018YFA0208600); 国家自然科学基金(22033003, 21533001, 91745201).
本文的电子版全文由Elsevier出版社在ScienceDirect上出版(http://www.sciencedirect.com/journal/chinese-journal-of-catalysis).